Langmuir
Article
pubs.acs.org/Langmuir

Photocurrent Generation from $Ru(bpy)_3^{2+}$ Immobilized on Phospholipid/Alkanethiol Hybrid Bilayers

Kai Jiang, Hong Xie, and Wei Zhan*

Department of Chemistry and Biochemistry, Auburn University, Auburn, Alabama 36849

Received April 30, 2009. Revised Manuscript Received June 30, 2009

A new photocurrent-generation system based on $Ru(bpy)_3^{2+}$ (bpy = 2,2′-bipyridine) tethered on phospholipid/alkanethiol hybrid bilayers in aqueous media is reported. The construction of such a system is straightforward. First, a self-assembled monolayer (SAM) of alkanethiol is formed on gold, and separately, liposomes containing $Ru(bpy)_3^{2+}$-conjugated dioleoylphosphoethanolamine (DOPE) are prepared by extrusion. Subsequent exposure of the $Ru(bpy)_3^{2+}$-containing liposome solution to the preformed SAM induces the addition of a monolayer of phospholipids on top of the SAM and thereby the immobilization of a $Ru(bpy)_3^{2+}$ layer on the gold electrode. Either anodic or cathodic photocurrent generation can be obtained, when ascorbate (anodic) or methyl viologen/oxygen (cathodic) is used as a sacrificial electron donor/acceptor, respectively. Light conversion quantum efficiencies of 0.84% (anodic) and 0.21% (cathodic) were obtained under blue light ($\lambda = 470 \pm 20$ nm) irradiation. The photocurrent-generation and electron-transfer mechanisms of this new system as well as its potential usefulness in fundamental photoconversion studies are discussed.

Introduction

We report herein a new photocurrent-generation system based on $Ru(bpy)_3^{2+}$ (bpy = 2,2′-bipyridine) tethered on phospholipid/alkanethiol hybrid bilayers in aqueous media. The construction of such a system comprises two steps (Scheme 1). First, a self-assembled monolayer (SAM) of alkanethiol is formed on gold, and separately, liposomes containing $Ru(bpy)_3^{2+}$-conjugated dioleoylphosphoethanolamine (DOPE) are prepared by extrusion. Subsequent exposure of the $Ru(bpy)_3^{2+}$-containing liposome solution to the preformed SAM induces the addition of a monolayer of phospholipids on top of the SAM and thereby the immobilization of a $Ru(bpy)_3^{2+}$ layer on the gold electrode. Either anodic or cathodic photocurrent generation can be obtained in the presence of a suitable sacrificial electron donor/acceptor. Conventional monolayer-based photoconversion systems[1−3] typically rely on the covalent linkage of thiol- or silane-functionalized photoactive conjugates on electrodes, which often require nontrivial synthesis in organic media. By contrast, the method described here takes advantage of the versatile assembly[4,5] of phospholipids in water and potentially provides a new approach to modular photoelectrochemical cell design.

Natural as well as synthetic lipids have long been employed as general building blocks in many research areas owing to their ability to assemble into stable, well-defined microscopic structures. In the studies of artificial photosynthesis and biomimetic photoconversion systems, bilayer structures based on lipid vesicles and black lipid membranes (BLMs) have been established as the primary experimental models.[6−10] When lipid vesicles are used, for example, the closed spherical lipid bilayer allows different redox species or the same species at different concentrations to be separated, thus producing a heterogeneous electrochemical distribution across the lipid bilayer. The occurrence of photoelectrochemical reactions can then be followed spectroscopically. In the case of BLMs, a lipid bilayer is formed inside a small hole on a Teflon sheet partitioning two sample chambers, which then enables photocurrents and photovoltages to be measured via two reference electrodes. In both systems, the photoactive agent can be placed either on the surface or in the interior of the lipid bilayer. Efficient photoconversion following the initial photoinduced electron transfer has often been observed because the lipid bilayer can act as an effective barrier to suppress the unwanted charge recombination.

In a separate lipid-based photoconversion system[11] we reported recently, a symmetrical lipid bilayer structure was used to fix photoactive fullerenes on an indium tin oxide electrode. Although this system generally functions satisfactorily in the single-(photoactive)component photocurrent generation processes, it provides only limited options for directional placement of multiple photoactive agents across the lipid bilayer, which is essential to achieving efficient vectorial electron transfer and photocurrent generation. In this regard, the hybrid-bilayer-based system illustrated here offers interesting new possibilities because the two monolayers are added onto the electrode surface in a sequential fashion and each layer can be separately modified.

Results and Discussion

Characterization of Hybrid Bilayers. Quartz crystal microbalance (QCM), cyclic voltammetry (CV), and impedance analysis were employed to characterize the formation and

*Corresponding author: E-mail: wzz0001@auburn.edu. Tel: 334-844-6984. Fax: 334-844-6959.

(1) Imahori, H.; Yamada, H.; Nishimura, Y.; Yamazaki, I.; Sakata, Y. *J. Phys. Chem. B* **2000**, *104*, 2099–2108.
(2) Terasaki, N.; Akiyama, T.; Yamada, S. *Langmuir* **2002**, *18*, 8666–8671.
(3) Matsuo, Y.; Kanaizuka, K.; Matsuo, K.; Zhong, Y.-W.; Nakae, T.; Nakamura, E. *J. Am. Chem. Soc.* **2008**, *130*, 5016–5017.
(4) Sackmann, E. *Science* **1996**, *271*, 43–48.
(5) Lasic, D. D. *Trends Biotechnol.* **1998**, *16*, 307–321.
(6) Gust, D.; Moore, T. A. *Top. Curr. Chem.* **1991**, *159*, 103–151.
(7) Gust, D.; Moore, T. A.; Moore, A. L. *Acc. Chem. Res.* **2001**, *34*, 40–48.
(8) Ford, W. E.; Otvos, J. W.; Calvin, M. *Proc. Natl. Acad. Sci. U.S.A.* **1979**, *76*, 3590–3593.
(9) Fendler, J. H. *Acc. Chem. Res.* **1980**, *13*, 7–13.
(10) Lymar, S. V.; Parmon, V. N.; Zamaraev, K. I. *Top. Curr. Chem.* **1991**, *159*, 1–65.
(11) Zhan, W.; Jiang, K. *Langmuir* **2008**, *24*, 13258–13261.

Scheme 1. Formation of $Ru(bpy)_3^{2+}$-Conjugated Phospholipid/Alkanethiol Hybrid Bilayers

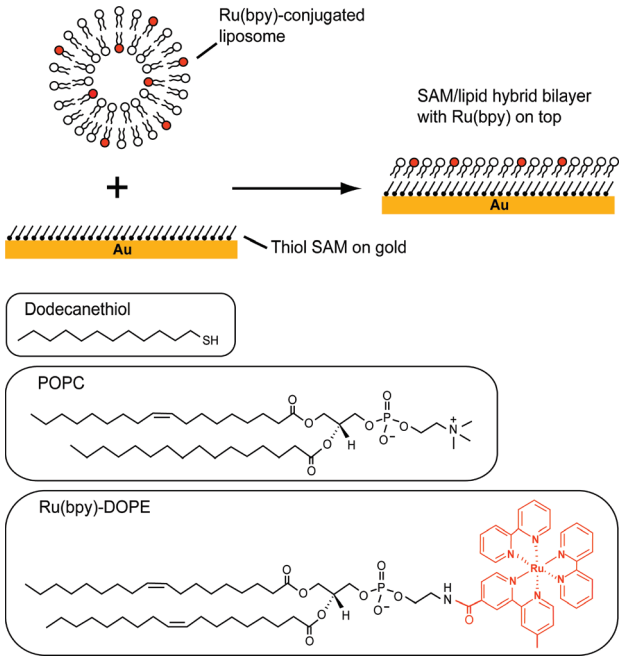

structure of the phospholipid/alkanethiol hybrid bilayers on gold substrates.

The stepwise deposition of the alkanethiol and phospholipid monolayer on gold was monitored by QCM. Here, the associated mass change of the quartz crystal corresponds to its oscillation frequency change according to the Sauerbrey equation[12]

$$\Delta f = -C_f \Delta m$$

where Δf is the observed frequency shift (Hz), Δm is the change in mass per unit area (g/cm^2), and C_f is the sensitivity factor for the crystal (i.e., 56.6 Hz μg^{-1}cm^2 for a 5 MHz AT-cut quartz crystal at room temperature). As shown in Figure 1, a 6.2 Hz frequency decrease was observed immediately after the 1-dodecanethiol was injected into the QCM chamber. This frequency shift corresponds to a thiol coverage of 3.2×10^{14} molecules/cm^2, which is lower than an ideal SAM coverage on gold (i.e., 4.16×10^{14} molecules/cm^2).[13] When the same calculation was performed for the formation of a POPC monolayer on top of the C12 SAM, a coverage of 3.65×10^{14} molecules/cm^2 was obtained. This value was significantly higher than that for the ideal lipid monolayer of 1.43×10^{14} molecules/cm^2, assuming the unit area per POPC molecule is 70 Å^2. Several factors might contribute to these apparent mismatches. For example, the Sauerbrey equation is known to be inadequate in the interpretation of liquid-based QCM results, in which case viscoelastic effects arising from the solvent and the adsorbed layers become significant.[12,14] Also, water molecules entrapped within the polar portion of the lipid layer[15] may contribute to the observed frequency shift.

Because alkanethiol and lipid thin films can effectively block electron transfer, their formation on a conducting surface can be

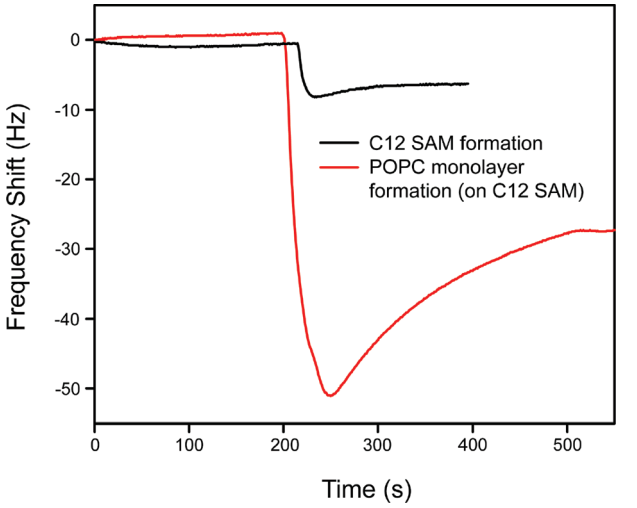

Figure 1. QCM monitoring of the formation of a C12 thiol SAM and sequentially a POPC/C12 SAM hybrid bilayer on gold. To form the top phospholipid layer, liposomes of POPC in 10 mM HEPES buffer saline (0.1 M NaCl, pH 7.7) solution were injected into the QCM flow cell. The estimated final concentrations of 1-dodecanethiol and POPC were 1 and 0.1 mM, respectively. See the Experimental Section for more details.

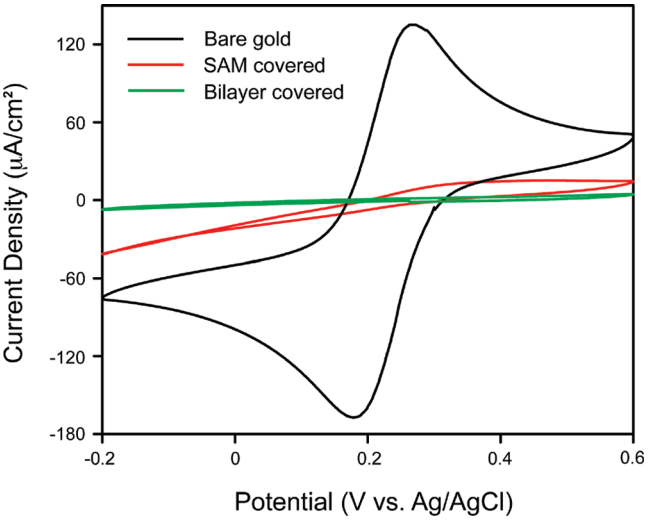

Figure 2. Electrochemical diagnosis of the formation of a C12 SAM and a POPC/C12 SAM hybrid bilayer on gold. To do this, cyclic voltammetry of 1 mM $Fe(CN)_6^{3-}$ in 1 M KCl was carried out using gold substrates covered with a C12 SAM alone or a C12 SAM/POPC bilayer. A three-electrode setup with a Ag/AgCl reference electrode and a Pt counter electrode was used. Scan rate: 50 mV/s.

followed electrochemically.[16,17] Figure 2 collects cyclic voltammograms of $Fe(CN)_6^{3-}$ probed by gold electrodes covered with a C12 SAM or a POPC/SAM bilayer in 1 M KCl solution. Clearly, the presence of a C12 SAM significantly diminishes the reduction/oxidation of $Fe(CN)_6^{3-}/Fe(CN)_6^{4-}$ on the gold electrode, and further addition of a POPC monolayer almost completely blocks the flow of a faradaic current within this potential window. These results thus indicate the formation of a well-packed C12 SAM and a POPC/SAM hybrid bilayer on gold surfaces.

Impedance spectroscopy results reveal the capacitance change associated with the formation of a thiol monolayer (C6, C12, and C18) and a lipid/alkanethiol bilayer on gold substrates (Figure 3). As shown in Table 1, the C6 SAM displays the highest capacitance in this series, which can be attributed to the existence of packing

(12) Buttry, D. A.; Ward, M. D. *Chem. Rev.* **1992**, *92*, 1355–1379.
(13) Dubois, L. H.; Nuzzo, R. G. *Annu. Rev. Phys. Chem.* **1992**, *43*, 437–463.
(14) Karpovich, D. S.; Blanchard, G. J. *Langmuir* **1994**, *10*, 3315–3322.
(15) Griffith, O. H.; Dehlinger, P. J.; Van, S. P. *J. Membr. Biol.* **1974**, *15*, 159–192.
(16) Porter, M. D.; Bright, T. B.; Allara, D. L.; Chidsey, C. E. D. *J. Am. Chem. Soc.* **1987**, *109*, 3559–3568.
(17) Plant, A. L. *Langmuir* **1993**, *9*, 2764–2767.

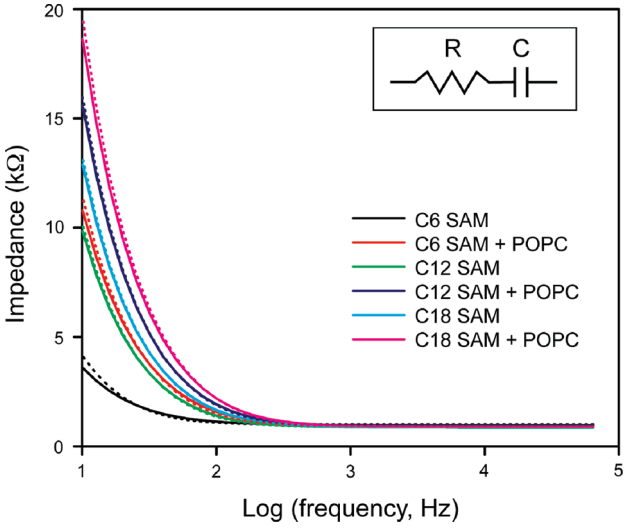

Figure 3. Impedance profile of SAMs (of C6-, C12-, and C18-thiol) and hybrid bilayers as a function of the applied ac frequency. A series RC circuit model is used to fit the resultant cell impedance in all measurements, and the fitted data are displayed by dotted lines. The supporting electrolytes contain 10 mM KCl in DI water.

Table 1. Effect of Different Alkanethiol SAM on the Capacitance of the Resulting POPC/Thiol Bilayers

	capacitance of the SAM layer (C_{SAM}: μF/cm^2)[a]	Capacitance of the bilayer ($C_{bilayer}$: μF/cm^2)[a]	capacitance of the lipid layer (C_{lipid}: μF/cm^2)[b]
C6	3.53	1.19	1.81
C12	1.35 ± 0.02[c]	0.85 ± 0.03[c]	2.31 ± 0.09[d]
C18	1.03	0.69	2.11

[a] Values are obtained by fitting the impedance data with a series-RC circuit model. [b] Calculated values. See the text for more details. [c] $n = 3$. [d] Calculated values.

Table 2. Effect of Different Amounts of Ru(bpy)$_3^{2+}$-DOPE on the Capacitance of the Resulting POPC/C12 SAM Bilayers

	capacitance of the bilayer ($C_{bilayer}$: μF/cm^2)[a]	capacitance of the lipid layer (C_{lipid}: μF/cm^2)[b]
1%[c]	0.81 ± 0.04[d]	2.06
2%[c]	0.86 ± 0.02[d]	2.37
3%[c]	0.89	2.66

[a] Values are obtained by fitting the impedance data with a series-RC circuit model. [b] Calculated values. [c] Amounts of Ru(bpy)$_3^{2+}$-DOPE included in the POPC layer. [d] $n = 3$.

defects in the film as well as its relatively small thickness. When a common POPC overlayer was used to form hybrid bilayers with these SAMs, the same trend was obtained. The capacitance of the lipid monolayer alone (C_{lipid}) can be calculated from the capacitance of the lipid/alkanethiol bilayer ($C_{bilayer}$) and the alkanethiol SAM layer (C_{SAM}) by the following equation:[17]

$$1/C_{lipid} = 1/C_{bilayer} - 1/C_{SAM}$$

Thus, the POPC layer exhibits the highest capacitance when a C12 SAM serves as the underlying layer, followed by that of C18 and C6. These results are in good agreement with that reported in a previous study.[18] Similar measurements were carried out for C12 SAM-based hybrid bilayers containing different amounts of

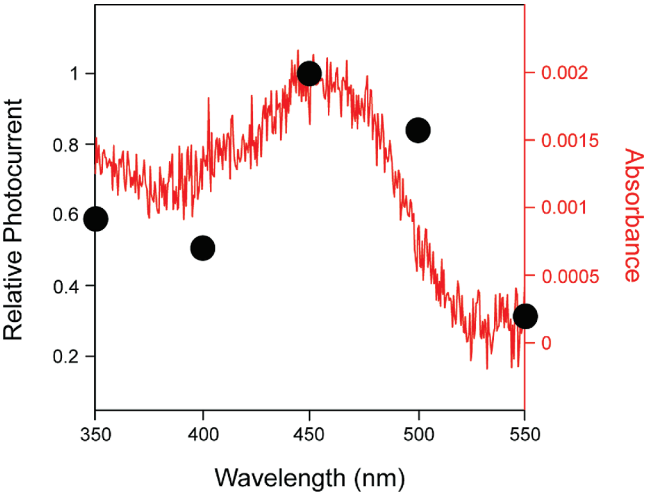

Figure 4. Photocurrent action spectrum obtained from POPC/C12 SAM hybrid bilayers containing 3% Ru(bpy)$_3^{2+}$-DOPE. Ascorbate (50 mM) was used as the sacrificial electron donor in 10 mM HEPES buffer saline (0.1 M NaCl, pH 7.7) solution, in which the oxygen was depleted by adding 50 mM glucose, 50 units/mL glucose oxidase, and 200 units/mL catalase. All photocurrents were measured against the cell open-circuit potentials (measured in the dark, typically -0.04 to -0.06 V (anodic) and 0.14 to 0.15 V (cathodic) vs Ag/AgCl). The trace in red is the corresponding UV−vis absorption spectrum obtained from two POPC lipid bilayers containing 3% Ru(bpy)$_3^{2+}$-DOPE coated on a clean glass substrate. See the Experimental Section for more details.

Ru(bpy)$_3^{2+}$-DOPE in the POPC top layer (Table 2). Here, the presence of increasing numbers of cationic lipids led to a gradual increase in capacitance in the lipid leaflets. As will be discussed in the following sections, this change of capacitance can strongly influence the observed photocurrents.

Photocurrent Generation. A series of experiments were carried out to understand the general behavior of the present photoconversion system based on the Ru(bpy)$_3^{2+}$-tethered hybrid bilayer, which includes (1) the dependence of photocurrents on light of different intensities and wavelengths, (2) the dependence of photocurrents on the light exposure time, (3) the dependence of photocurrents on the potential bias applied, and (4) the energetics associated with the anodic/cathodic photocurrent generation.

Figure 4 shows a preliminary photocurrent action spectrum in the range of 350−550 nm, which covers the metal-to-ligand charge-transfer (MLCT) region of Ru(bpy)$_3^{2+}$-based complexes.[19,20] The spectrum generally correlates with the UV−vis spectrum taken directly from the Ru(bpy)$_3^{2+}$-containing lipid bilayer formed on glass, indicating that excited-state Ru(bpy)$_3^{2+}$* is responsible for the observed photocurrent generation (see below).

A linear relationship between the incident light intensity and the resulting photocurrent was observed when the light intensity was varied from 3.1 to 31.1 mW/cm^2 (Figure 5a). Moreover, the photocurrents were also found to increase linearly with the increase in the electron mediator concentration up to ~100 mM (Figure 5b). At still higher ascorbate concentrations, the photocurrents follow the same trend but at a somewhat slower pace. These results indicate that the photocurrent generation is limited by the diffusion of the mediator molecules to the Ru(bpy)$_3^{2+}$-bound lipid surface.

(18) Silin, V. I.; Wieder, H.; Woodward, J. T.; Valincius, G.; Offenhausser, A.; Plant, A. L. *J. Am. Chem. Soc.* **2002**, *124*, 14676–14683.

(19) Kalyanasundaram, K. *Coord. Chem. Rev.* **1982**, *46*, 159–244.

(20) Juris, A.; Balzani, V.; Barigelletti, F.; Campagna, S.; Belser, P.; Vonzelewsky, A. *Coord. Chem. Rev.* **1988**, *84*, 85–277.

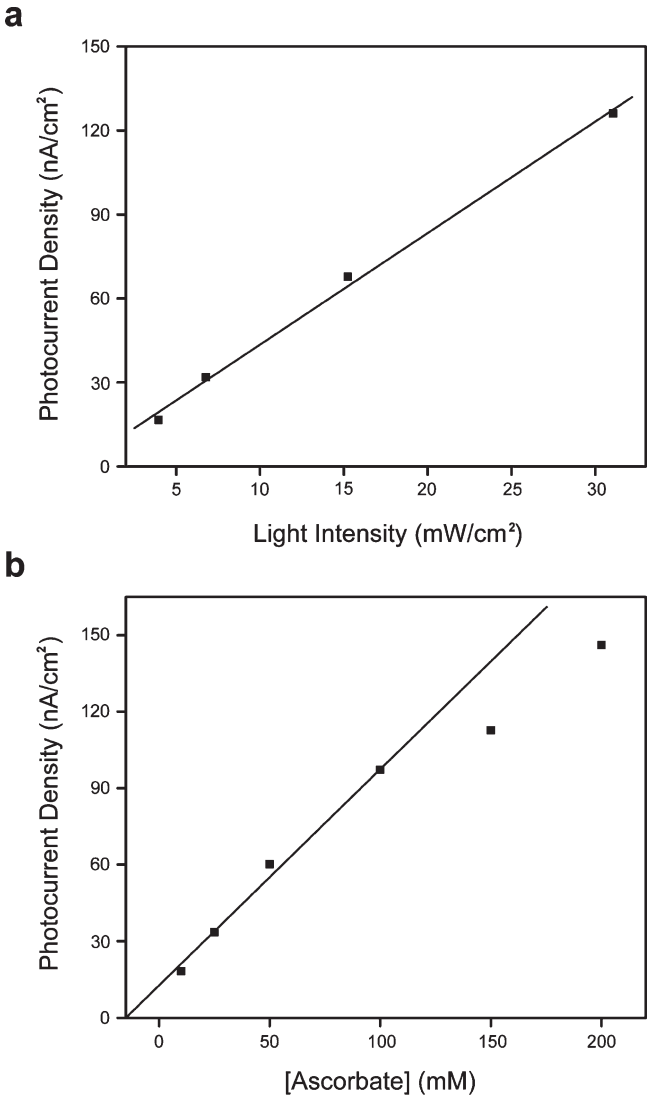

Figure 5. Photocurrent vs (a) the incident light intensity and (b) the sacrificial donor concentration. (a) The photocurrents were generated on a gold substrate covered with a POPC/C12 SAM hybrid bilayer containing 3% $Ru(bpy)_3^{2+}$-DOPE. (b) Photocurrents were generated on a gold substrate covered with a POPC/C12 SAM hybrid bilayer of 1% $Ru(bpy)_3^{2+}$-DOPE with various ascorbate concentrations. Light: 470 ± 20 nm. Other conditions are the same as in Figure 4.

Figure 6 shows that either anodic or cathodic photocurrent generation can be realized in this system, when ascorbate (anodic) and methyl viologen/oxygen (cathodic) are used as the sacrificial electron donor and acceptor, respectively. Moreover, for the cells based on 1% $Ru(bpy)_3^{2+}$-DOPE in the POPC/C12 SAM bilayer, a light-conversion quantum efficiency of 0.84(0.21)% could be determined in the anodic(cathodic) photocurrent generation (see the Experimental Section). Both processes are initiated by the photoexcitation of $Ru(bpy)_3^{2+}$, which produces a highly reactive electron/hole pair that can facilitate both reduction and oxidation at the electrode depending on the energy level of the redox species present in solution. Noticeably, the cathodic photocurrent generated measures only 25% of the anodic current, which might be due to several reasons. First, the apparent thermodynamic driving force (i.e., the potential difference associated with anodic electron-transfer processes) is about 800 mV higher than that of the cathodic case (Figure 6b), which eventually leads to a higher anodic photocurrent. Furthermore, compared to

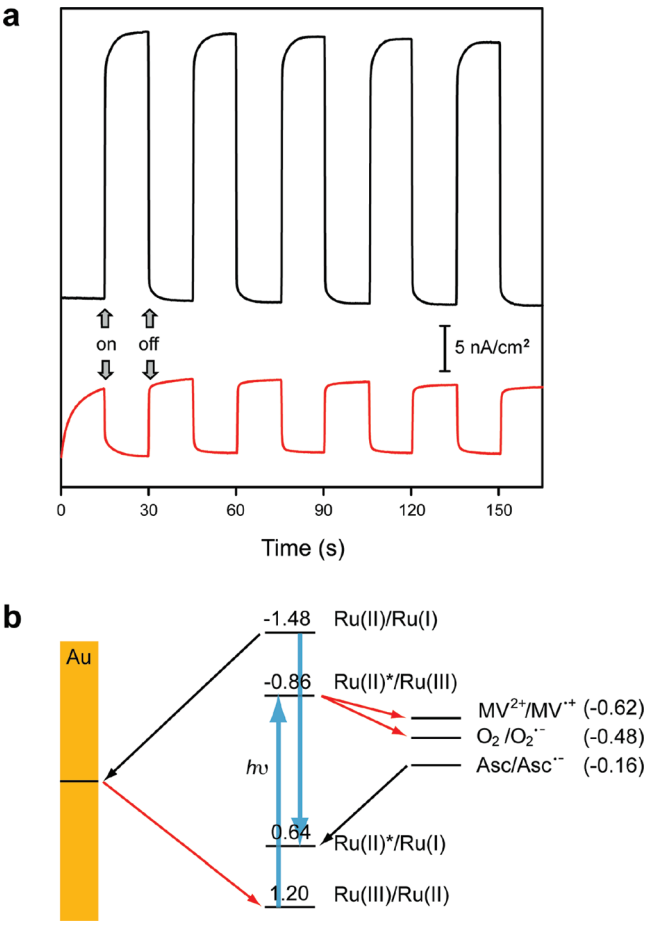

Figure 6. (a) Anodic (curve in black) vs cathodic (curve in red) photocurrents (taken after the initial decay, see Figure 8) from POPC/C12 SAM hybrid bilayers containing 1% $Ru(bpy)_3^{2+}$-DOPE. Experimental conditions for anodic photocurrent generation are identical to those described in Figure 4, whereas cathodic currents were obtained in 10 mM HEPES buffer saline (0.1 M NaCl, pH 7.7) containing 50 mM methyl viologen and air-saturated oxygen. (b) Electrochemical potentials of species involved in the photocurrent generation. All potentials are given vs Ag/AgCl. The electron-flow pathways are depicted by black(red) arrows for anodic(cathodic) photocurrent generation.

the reversible reduction of MV^{2+}/O_2 involved in the cathodic route, the oxidation of ascorbate in the anodic current generation directly leads to its decomposition. This irreversible process, therefore, greatly favors the forward electron transfer between ascorbate and $Ru(bpy)_3^{2+}$* by eliminating the competing charge recombination[21] between the two. Different redox intermediates are likely involved in the two photocurrent-generation pathways (Figure 6b). In the cathodic process, the excited $Ru(bpy)_3^{2+}$* species reduces MV^{2+} and O_2 and becomes $Ru(bpy)_3^{3+}$, which is then reduced back to $Ru(bpy)_3^{2+}$ heterogeneously by the gold electrode.[22,23] In the anodic route,[20,24] however, the excited $Ru(bpy)_3^{2+}$* is first reduced by ascorbate to $Ru(bpy)_3^{+}$, which then injects an electron into the electrode.

On the basis of the energetics and electron-transfer pathways involved in the anodic photocurrent generation, it can be derived

(21) Mauzerall, D. C. *Photoinduced Electron Transfer*; Fox, M. A., Chanon, M., Eds.; Elsevier Science Publishers B. V.: Amsterdam, The Netherlands, 1988; Part A, pp 207−244.
(22) Terasaki, N.; Akiyama, T.; Yamada, S. *Langmuir* **2002**, *18*, 8666–8671.
(23) Nitahara, S.; Akiyama, T.; Inoue, S.; Yamada, S. A *J. Phys. Chem. B* **2005**, *109*, 3944–3948.
(24) Sutin, N.; Creutz, C. *Adv. Chem. Ser.* **1978**, *168*, 1–27.

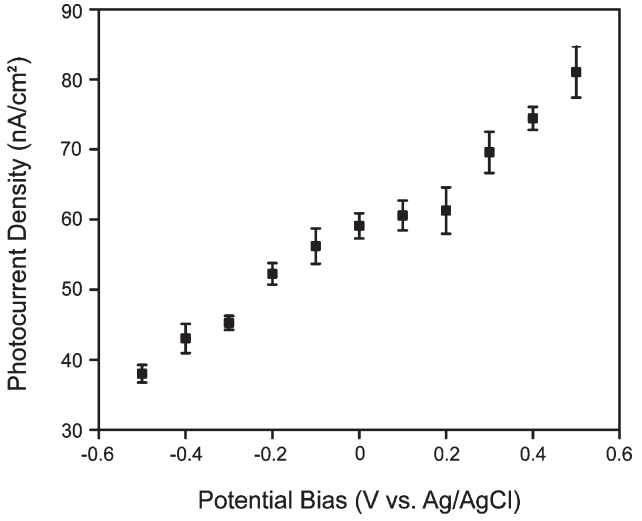

Figure 7. Effect of potential bias on the measured photocurrents. The lipid top layer contains 1% $Ru(bpy)_3^{2+}$-DOPE; measurements were carried out in 50 mM ascorbate in HEPES buffer saline free of oxygen. Data are averaged from three parallel experiments, and the error bars represent the standard deviation of the corresponding measurement.

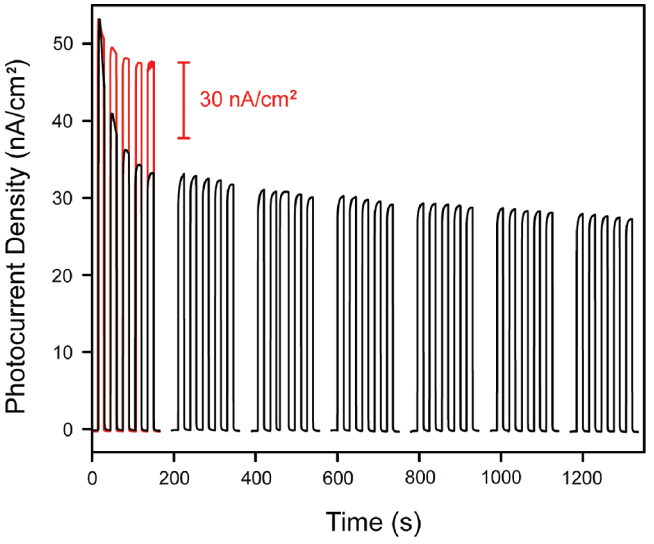

Figure 8. Photocurrent output as a function of photoexcitation time from POPC/C12 SAM hybrid bilayers containing 1% $Ru(bpy)_3^{2+}$-DOPE. Other conditions are the same as in Figure 4. The superimposed trace in red records the initial photocurrent decay when 200 mM ascorbate is used.

that a positive bias applied on the gold electrode will induce a higher photocurrent, whereas a negative bias will do the opposite. This trend is confirmed by the result shown in Figure 7.

Photocurrent decay was generally observed in the present photocurrent-generation system. As shown in Figure 8, the sharpest decay occurred immediately after the initial light excitation, which was followed by a slower decay upon further exposure. Over a period of 20 min of irradiation of the film with 15 s light pulses, a 43% decrease in photocurrent resulted. This decay, however, can be greatly reduced by increasing the ascorbate concentration in the solution (red trace, Figure 8). Presumably, the photogenerated $Ru(bpy)_3^{2+*}$ can react with some yet unidentified lipid moieties, which then leads to the degradation of the photoactive layer and thus the photocurrent decay. When a higher level of ascorbate is present, more $Ru(bpy)_3^{2+*}$ become directly scavenged, leaving less $Ru(bpy)_3^{2+*}$ available for the photodestructive reaction path. This result, therefore, indicates that it is $Ru(bpy)_3^{2+*}$ rather than $Ru(bpy)_3^{+}$ that causes the photocurrent decay in the anodic process. It should also be mentioned that photocurrent decays have been observed previously in lipid-based systems, e.g., a photoelectrochemical cell based on fullerenes embedded in a black lipid membrane.[25]

Photoinduced Electron Transfer across Hybrid Bilayers. It is important to understand how the photoinduced electron-transfer processes are initiated and sustained on a solid-supported phospholipid/thiol bilayer. Although discussions directly applicable to our system are not found in the literature, general observations obtained from previous lipid-based photoconversion studies[10,26] can serve as a good starting point.

Depending on the chemical composition and structural arrangement of the system, photoinduced electron transfer across lipid bilayers can follow either direct or mediated-transfer pathways. In the absence of an electron mediator, moreover, the direct electron-transfer pathway can proceed via either diffusion or electron-exchange based mechanisms or, to some extent, their combination. A mixed scenario has often been suggested because the fluidic and dynamic lipids allow translocation and the conformational change of photoactive species to occur within the matrix.[10,26] However, a transfer process based on electron tunneling is more favored for systems in which the lipid matrix is rigid (i.e., polymerized or gel-like lipids) or the photosensitizer is too bulky to move freely. In these cases, distance-dependent photocurrent generation is normally observed, and an effective tunneling distance of up to 40 Å has been proposed.[10]

The overall performance of this new photoelectrochemical cell depends on the distance between the photoactive species and the electrode and therefore the thickness of the constituent SAM and phospholipid layers. To study this distance dependence, three alkanethiols (C6-, C12-, and C18-thiol) were used to form the hybrid bilayers with a POPC top layer, and the resulting photocurrents taken after the initial decay were compared. As shown in Figure 9, relatively stable photocurrents were observed in all three cases. Moreover, an ~15% higher response was obtained when C12 SAM was the underlying layer, whereas photocurrents generated from hybrid bilayers with C6 and C18 SAMs were roughly comparable. Compared to thiols with relatively long alkane chains, C6-thiol is too short to form a well-packed SAM on gold,[16] which, in turn, prohibits the formation of a well-packed phospholipid overlayer. This explains why the hybrid bilayer based on the C12 SAM displays a higher photocurrent than that based on the C6 SAM; even though the $Ru(bpy)_3^{2+}$-to-electrode distance is likely smaller in the latter case, its relatively lower $Ru(bpy)_3^{2+}$ surface coverage affords a smaller photocurrent. However, whereas a similarly well packed lipid monolayer is expected to form on both C12 and C18 SAMs, $Ru(bpy)_3^{2+}$ complexes are placed further away from the electrode when the C18 SAM serves as the base layer. This results in a weakened electron-tunneling process and thus a smaller photocurrent.

It is possible to estimate the apparent electrical thickness (d) of the POPC top layer from the calculated capacitance values using the following relationship[17]

$$1/C = d/\varepsilon\varepsilon_0$$

(25) Hwang, K. C.; Mauzerall, D. *Nature* **1993**, *361*, 138–140.
(26) Baral, S.; Fendler, J. H. In *Photoinduced Electron Transfer*; Fox, M. A., Chanon, M., Eds.; Elsevier Science Publishers B. V.: Amsterdam, The Netherlands, 1988; Part B, pp 541−598.

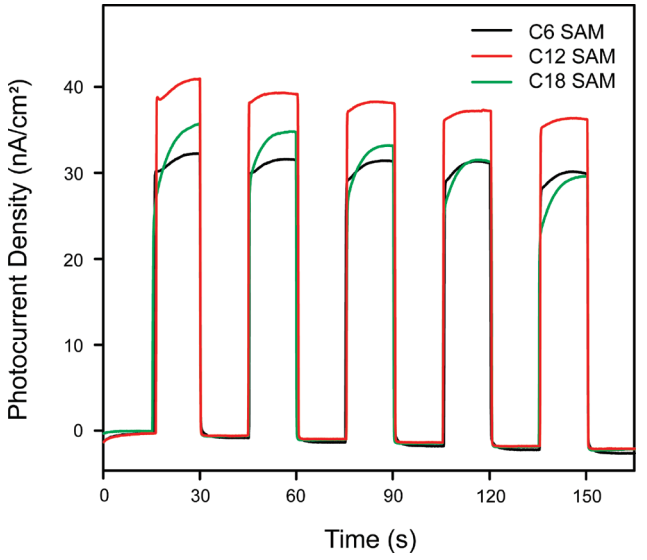

Figure 9. Effect of different alkanethiols on the obtained photocurrents. SAMs of C6-, C12-, and C18-thiol were formed by immersing clean gold substrates in 1 mM thiol solutions in ethanol for at least 12 h. In each case, a POPC monolayer containing 1% $Ru(bpy)_3^{2+}$-DOPE was formed on top of the SAM. Fifty millimolar ascorbate was used as the sacrificial electron donor in 10 mM HEPES buffer saline (0.1 M NaCl, pH 7.7) solution depleted of oxygen.

Table 3. Calculated Thickness of the Alkanethiol SAM and Lipid Layers[a]

	thickness of the SAM layer (nm)	thickness of the POPC lipid layer (nm)
C6	0.58	1.32
C12	1.51	1.03
		1.16 (1%)[b]
		1.01 (2%)[b]
		0.90 (3%)[b]
C18	1.98	1.13

[a] ε values of 2.3 and 2.7 were used for alkanethiol and POPC monolayers in the calculation.[18] [b] Amounts of $Ru(bpy)_3^{2+}$-DOPE included in the POPC layer.

provided that the dielectric constant (ε) and the capacitance (C) of the material are known. As shown in Table 3, the thickness of the POPC layers tends to vary depending on the underlying SAMs. The thinnest POPC layer is obtained when a C12 SAM is employed as the base, which again agrees with what is observed by Silin and co-workers.[18] Noticeably, a significantly larger lipid layer thickness (i.e., 1.32 nm) was obtained in the case of the C6 SAM, which is likely due to the poor packing and low ordering of the lipid/C6 SAM bilayer that can lower the accuracy of the estimation. Additionally, when $Ru(bpy)_3^{2+}$-DOPE was added to POPC to form a mixed lipid top layer, the measured capacitance increased with the amount of $Ru(bpy)_3^{2+}$-DOPE included (Table 2). Assuming that the presence of $Ru(bpy)_3^{2+}$-DOPE does not affect the dielectric constant of the resulting lipid layers,[27,28] it can be concluded that $Ru(bpy)_3^{2+}$-DOPE can reduce the electrical thickness of the lipid layer on the C12 SAM (Table 3). For example, a thickness of 0.90 nm was obtained for a POPC layer containing 3% $Ru(bpy)_3^{2+}$-DOPE, as compared to 1.03 nm from the lipid layer of POPC alone. This thickness decrease can be

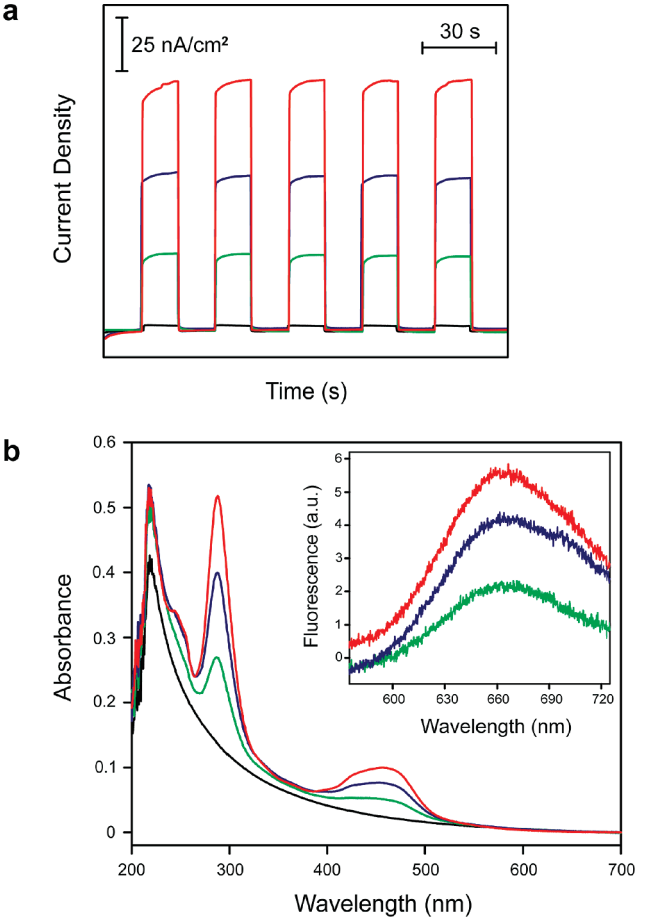

Figure 10. Photocurrent vs $Ru(bpy)_3^{2+}$-DOPE loading in the phospholipid layer. (a) In each case, the photocurrents were taken after the initial decay over the same period. Other conditions are the same as in Figure 4. (b) UV spectra (from bottom to top) are obtained from 0.25 mM POPC liposome solutions containing 0, 1, 2, and 3% $Ru(bpy)_3^{2+}$-DOPE in 10 mM HEPES buffer saline (0.1 M NaCl, pH 7.7) solution. The inset records the corresponding fluorescence emission spectra obtained from $Ru(bpy)_3^{2+}$-linked lipid monolayers (1−3%, from bottom to top) formed on gold substrates. See the text for more details.

understood as follows: (1) The unsaturated dioleoyl chain in DOPE ($T_m = -16$ °C) further increases the degree of disorder of the POPC ($T_m = -9$ °C) layer and therefore lowers the apparent thickness of the mixed lipid layer. (2) The hydrophilic, bulky $Ru(bpy)_3^{2+}$ moieties in the headgroup region of the lipid layer enlarge the penetration depth of water and ionic molecules into the lipid matrix, again resulting in a decrease in the apparent thickness of the mixed lipid layer.

The above results obtained from impedance analysis enable us to correlate the measured photocurrents with the thickness of the hybrid bilayers and thus the electron-tunneling distance. Whereas higher loadings of $Ru(bpy)_3^{2+}$ in the lipid layer generally lead to higher photocurrents, a disproportionally larger current is obtained for the cell containing 3% $Ru(bpy)_3^{2+}$ (Figure 10a). Clearly, this extra increase in photocurrent arrives from the electrically thinner lipid layer induced by the presence of 3% $Ru(bpy)_3^{2+}$-DOPE, which allows electron transfer to occur more efficiently. Notice that this increase is not due to a higher loading of photoactive species in the film containing 3% $Ru(bpy)_3^{2+}$-DOPE, since the absorption/fluorescence spectroscopy data indicate that the amount of surface-immobilized $Ru(bpy)_3^{2+}$ varies almost linearly with its starting concentration in liposomes (Figure 10b).

(27) Benz, R.; Frohlich, O.; Lauger, P.; Montal, M. *Biochim. Biophys. Acta* **1975**, *394*, 323–334.
(28) Alvarez, O.; Latorre, R. *Biophys. J.* **1978**, *21*, 1–17.

A combined mechanism including both diffusional and electron-tunneling processes can be proposed to account for the $Ru(bpy)_3^{2+}$-to-electrode electron transfer in the present system. Here, the hybrid bilayer yields a total electrical thickness of < 3 nm, which should allow electrons to tunnel directly from the top of the bilayer. In addition, $Ru(bpy)_3^{2+}$-DOPE lipids may also undergo some conformational change through the bending of the DOPE headgroup within the lipid layer. These lipid-associated $Ru(bpy)_3^{2+}$ complexes can still bridge the electron-transfer path in the bilayer by taking electrons from the surface-oriented $Ru(bpy)_3^{2+}$ species via the electron-tunneling-based exchange mechanism.[8,10] This conformational change is considered to be possible here because (1) the mixed POPC/DOPE layer is very disordered and fluidic, (2) $Ru(bpy)_3^{2+}$ exhibits high solubility in both organic and aqueous media,[29] and (3) upon photoexcitation, $Ru(bpy)_3^{2+*}$ is reduced by ascorbate to $Ru(bpy)_3^{+}$, which should experience a lowered barrier moving toward the hydrophobic region of the lipids. Further research is needed to determine if this is indeed the case.

Conclusions

We have demonstrated here a new photocurrent-generation system constructed on phospholipid/alkanethiol hybrid bilayers. This system exhibits important technical advantages over that based on symmetrical lipid bilayers[11] in that the two monolayers are added onto the electrode surface sequentially and the chemical/electrical properties of each layer can be separately tailored to achieve a higher performance. A number of strategies can be added to the present system to enhance the photoconversion efficiency, for example, multicomponent systems containing multiple photosensitizing and antenna species and further improvements in the electron-transfer paths across the bilayer using electrically conducting SAMs. Investigations along these lines are currently underway in this laboratory.

Experimental Section

Reagents. Phospholipids such as 1-palmitoyl-2-oleoyl-*sn*-glycero-3-phosphocholine (POPC) and 1,2-dioleoyl-*sn*-glycero-3-phosphoethanolamine (DOPE) were obtained from Avanti Polar Lipids. Potassium hexacyanoferrate(III) ($K_3Fe(CN)_6$) was from Riedel-de Haen. Other chemicals, including bis(2,2′-bipyridine)-4′-methyl-4-carboxybipyridine-ruthenium *N*-succinimidyl ester-bis(hexafluorophosphate), ($Ru(bpy)_3^{2+}$-NHS), *N,N*-dimethylformamide (DMF), triethylamine, 1-hexanethiol, 1-dodecanethiol, 1-octadecanethiol, 4-(2-hydroxyethyl)piperazine-1-ethanesulfonic acid (HEPES), methyl viologen dichloride hydrate (MV^{2+}), L(+)-ascorbic acid sodium salt (sodium ascorbate), D-(+)-glucose, glucose oxidase (type X-S, from *Aspergillus niger*), and catalase from bovine liver were purchased from Sigma-Aldrich. All solutions employed in these experiments were prepared using 18.2 MΩ cm deionized water (Millipore).

Synthesis of $Ru(bpy)_3^{2+}$-DOPE. $Ru(bpy)_3^{2+}$-DOPE was made in one step by reacting $Ru(bpy)_3^{2+}$-NHS with DOPE. To start, 2.5 μmol of DOPE in chloroform was added to a flask and dried with an argon stream, to which 0.8 mL of DMF and 25 μmol of triethylamine were added and stirred for 30 min. Next, 5 μmol of $Ru(bpy)_3^{2+}$-NHS in DMF was injected into the flask and thoroughly mixed. The final reaction volume was close to 1 mL. The reaction proceeded overnight at room temperature in the dark. The resulting products were dried and separated on a silica gel column (200−400 mesh) using chloroform and chloroform/methanol/water (90:10:0.5 and then 65:25:4 v/v/v). The production of $Ru(bpy)_3^{2+}$-DOPE was confirmed by TLC, ^{1}H NMR (in $CDCl_3$, see the Supporting Information), and EIS-MS (calculated, 1353.7; found, 1354).

Assembly of Hybrid Bilayers. Gold-coated substrates were fabricated by sputtering gold onto chromium-coated silicon wafers. The thickness of the gold layer was about 1000 nm. Prior to the self-assembly of alkanethiol monolayers, the gold-coated substrates were cleaned in piranha solution (3:1 v/v concentrated H_2SO_4/30% H_2O_2 solution) for 15 min and thoroughly rinsed with water and ethanol and dried in an argon stream. (***Caution! Piranha solution can react violently with organic materials and should be handled with extreme care***.) Thus-cleaned gold electrodes were incubated in 1 mM alkanethiol in ethanol solution at room temperature for at least 12 h. After that, the SAM-modified gold substrates were rinsed with copious amounts of ethanol and DI water, dried in argon, and then assembled in the Teflon photoelectrochemical cell for further use.

The preparation of liposomes has been described previously.[11] To form the phospholipid/alkanethiol hybrid bilayer, 300 μL of liposome solution, with a total lipid concentration of 2.5 mM, was added to the Teflon cell and incubated for 2 h. The unbound liposome solution was then removed from the cell by exchanging with HEPES buffer solution (10 mM HEPES, 100 mM NaCl, pH 7.7) at least 10 times.

Impedance Analysis. The impedance of the alkanethiol monolayer and lipid/alkanethiol hybrid bilayer was measured with an SI 1260 impedance/gain-phase analyzer (Solartron). The measurements were carried out on a two-electrode setup (Au working electrode and Pt counter electrode) in 10 mM KCl. A sinusoidal ac amplitude of 10 mV versus the open-circuit potential was applied throughout the measurements. An impedance analysis software package, ZView, was employed to fit the impedance data, which is based on an equivalent circuit consisting of a resistor (the electrolyte solution) and a capacitor (the surface-bound layers) connected in series.

QCM Measurements. QCM measurements were carried out using a QCM analyzer with a 5 MHz crystal oscillator (model QCM25, Stanford Research Systems) at 23 °C. Prior to SAM formation, the gold-coated quartz crystals were cleaned in piranha solution for 3 min and then rinsed with copious amounts of water and ethanol and dried under argon. The crystals were mounted onto the QCM oscillator equipped with a flow cell. To monitor SAM formation using QCM, ethanol was first flowed through the cell until a steady baseline of frequency was obtained. Following that, a proper amount of 100 mM dodecanethiol in ethanol was injected into the flow cell so that a final thiol concentration of 1 mM was obtained. For hybrid bilayer formation, the cleaned crystal was first immersed in 1 mM C12-thiol in ethanol overnight, thoroughly rinsed with ethanol and water, and finally dried in argon. To introduce POPC liposome solution into the cell, liposome solutions were injected into the QCM chamber pre-equilibrated with HEPES buffer. The final lipid concentration was about 0.1 mM.

Fluorescence Spectroscopy. The fluorescence emission spectra of the $Ru(bpy)_3^{2+}$-containing hybrid bilayer on semitransparent gold-coated glass slides were acquired using a PI Acton spectrometer (SpectraPro SP 2356, Acton, NJ) that is connected to the side port of an epifluorescence microscope (Nikon TE-2000U, Japan). The emission signal was recorded by a back-illuminated digital CCD camera (PI Acton PIXIS:400B, Acton, NJ) operated by a PC. The excitation was generated by a mercury lamp (X-Cite 120, EXFO, Ontario, Canada) filtered by a band-pass filter at 470 ± 20 nm. The emission signal was filtered by a long-pass filter with a cutoff wavelength of 515 nm.

Electrochemical and Photoelectrochemical Measurements. The electrochemical and photoelectrochemical measurements were carried out in a three-electrode Teflon photoelectrochemical cell. The three-electrode setup contains the gold substrate (with/without SAM or a lipid/SAM bilayer) as the working electrode and Pt and Ag/AgCl (KCl-saturated) as the counter

(29) Zhan, W.; Bard, A. J. *Anal. Chem.* **2006**, *78*, 726–733.

electrode and reference electrode. The effective area of the gold electrode is 1.13 cm^2. The cyclic voltammetry experiments were conducted with a potentiostat (CHI 910B, CH Instruments) in 1 mM potassium hexacyanoferrate(III) in 1 M KCl, and the scan rate was 50 mV/s.

In the photoelectrochemical measurements, the electrolytes contain either 50 mM ascorbate (cathodic) or methyl viologen (anodic) in HEPES buffer. The cell was irradiated with light from a Hg lamp (X-Cite, series 120 PC, EXFO) filtered at 470 ± 20 nm (average intensity, 26.8 mW/cm^2). In the case of anodic current generation, oxygen in the cell was removed by an enzymatic method reported previously.[23] The resulting photocurrent was recorded by a potentiostat (CHI 910B, CH Instruments). The photoconversion efficiency was calculated according to $\Phi = (i/e)/[(W\lambda/hc)(1-10^{-A})]$, where i is the measured photocurrent, e is the elementary charge, W is the light power at wavelength λ, h is Planck's constant, c is the speed of light, and A is the absorbance of $Ru(bpy)_3^{2+}$-DOPE in the hybrid bilayer at 470 nm. The absorbance (A) of $Ru(bpy)_3^{2+}$-DOPE in the bilayer at 470 nm, 1.5×10^{-4}, was estimated by averaging the total absorbance from multiple layers formed on glass slides. The gold surface reflectance[30] of 0.34 was used to correct the light reflection by gold and its subsequent reabsorption by the photoactive layers.

(30) *Handbook of Optics*, 2nd ed.; Bass, M., Van Stryland, E. W., Wolfe, W. L., Eds.; McGraw-Hill: New York, 1995; Vol. *II*.

Acknowledgment. This work is supported by Auburn University and the USDA (through AUDFS). We thank Prof. Jeffery Fergus for providing access to an impedance analyzer. We also thank Prof. Peter Livant, Chengdong Huang, and Xiaoxun Li for their help with the NMR analysis.

Supporting Information Available: ^1H NMR spectra of $Ru(bpy)_3^{2+}$-DOPE. This material is available free of charge via the Internet at http://pubs.acs.org.